











RESEARCH ARTICLE

10.1029/2021JD036105

Using Ice Cores to Evaluate CMIP6 Aerosol Concentrations Over the Historical Era

Key Points:

- The sulfate ice-core increase until 1970 and its subsequent decrease is well depicted by models
- The post-1950 increase of black carbon (BC) predicted by models is not confirmed by ice-core trends showing instead an early 20th century maximum
- Ice cores reveal possible errors in Coupled Model Intercomparison Project Phase 6 emission inventories of BC in Europe

Kine Onsum Moseid^{1,2,3} , **Michael Schulz**^{1,2} , **Anja Eichler**^{4,5} , **Margit Schwikowski**^{4,5,6} , **Joseph R. McConnell**⁷ , **Dirk Olivie'**¹, **Alison S. Criscitiello**⁸ , **Karl J. Kreutz**^{9,10} , and **Michel Legrand**^{11,12} 

¹Norwegian Meteorological Institute, Research Department, Oslo, Norway, ²Department of Geoscience, University of Oslo, Oslo, Norway, ³Expert Analytics, Oslo, Norway, ⁴Laboratory of Environmental Chemistry, Paul Scherrer Institute, Villigen, Switzerland, ⁵Oeschger Centre for Climate Change Research, University of Bern, Bern, Switzerland, ⁶Department of Chemistry and Biochemistry, University of Bern, Bern, Switzerland, ⁷Division of Hydrologic Sciences, Desert Research Institute, Reno, NV, USA, ⁸Department of Earth and Atmospheric Sciences, University of Alberta, Edmonton, AB, Canada, ⁹School of Earth and Climate Sciences, University of Maine, Orono, ME, USA, ¹⁰Climate Change Institute, University of Maine, Orono, ME, USA, ¹¹Université Grenoble Alpes, CNRS, Institut des Géosciences de l'Environnement (IGE), Grenoble, France, ¹²Laboratoire Interuniversitaire des Systèmes Atmosphériques, Université de Paris and University Paris Est Creteil, CNRS, LISA, France

Correspondence to:

K. O. Moseid,
komoseid@gmail.com

Citation:

Moseid, K. O., Schulz, M., Eichler, A., Schwikowski, M., McConnell, J. R., Olivie', D., et al. (2022). Using ice cores to evaluate CMIP6 aerosol concentrations over the historical era. *Journal of Geophysical Research: Atmospheres*, 127, e2021JD036105. <https://doi.org/10.1029/2021JD036105>

Received 26 OCT 2021
Accepted 26 AUG 2022

Author Contributions:

Conceptualization: Michael Schulz

Data curation: Anja Eichler, Margit Schwikowski, Joseph R. McConnell, Alison S. Criscitiello, Karl J. Kreutz, Michel Legrand

Methodology: Michael Schulz, Dirk Olivie'

Software: Dirk Olivie'

Supervision: Michael Schulz

Writing – review & editing:

Michael Schulz, Anja Eichler, Margit Schwikowski, Joseph R. McConnell, Alison S. Criscitiello, Michel Legrand

Abstract The radiative effect of anthropogenic aerosols is one of the largest uncertainties in Earth's energy budget over the industrial period. This uncertainty is in part due to sparse observations of aerosol concentrations in the pre-satellite era. To address this lack of measurements, ice cores can be used, which contain the aerosol concentration record. To date, these observations have been under-utilized for comparison to aerosol concentrations found in state-of-the-art Earth system models (ESMs). Here we compare long term trends in concentrations of sulfate and black carbon (BC) between 15 ice cores and 11 ESMs over nine regions around the world during the period 1850–2000. We find that for sulfate concentration trends model results generally agree with ice core records, whereas for BC concentration the model trends differ from the records. Absolute concentrations of both investigated species are overestimated by the models, probably in part due to representation errors. However, we assume that biases in relative trends are not altered by these errors. Ice cores in the European Alps and Greenland record a maximum BC concentration before 1950, while most ESMs used in this study agree on a post-1950 maximum. We source this bias to an error in BC emission inventories in Europe. Emission perturbation experiments using NorESM2-LM support the observed finding that BC concentrations in Northern Greenland ice cores are recording European emissions. Errors in BC emission inventories have implications for all future and past studies where Coupled Model Intercomparison Project Phase 6 historical simulations are compared to observations relevant to aerosol forcing.

1. Introduction

Aerosols and aerosol precursors are both naturally and anthropogenically emitted into the atmosphere, and their total effect on climate is primarily by cooling the surface and thereby counteracting global warming (Forster et al., 2021; Lohmann & Feichter, 2005; Storelvmo et al., 2016). However, the historical aerosol forcing is highly uncertain (Forster et al., 2016; Schulz et al., 2006), both due to sparse aerosol observations in the pre-satellite era and our lack of understanding of aerosol microphysical processes (Lohmann, 2017). Constrained historical aerosol forcing estimates would allow ultimately for a better quantification of climate sensitivity (Bellouin et al., 2019; Bender, 2020), which is a key parameter in climate science (Sherwood et al., 2020).

Glaciers act as archives for deposited aerosols, and ice cores allow for the evaluation of aerosol concentration trends in the near and far past. Even though previous studies have compared ice core data to atmospheric models (Bauer et al., 2013; Engardt et al., 2017; Fagerli et al., 2007) they are an under-utilized source for Earth system model (ESM) evaluation.

ESMs are commonly used as a numerical tool for carrying out experiments to determine for instance aerosol forcing and climate sensitivity. The reconstruction of historical climate evolution by an ESM depends among other factors on the external forcing, and of specific interest in this work, the evolution of aerosol emissions. Within the Coupled Model Intercomparison Project Phase 6 (CMIP6) (Eyring et al., 2016), a large number of ESMs were

© 2022. The Authors.

This is an open access article under the terms of the [Creative Commons Attribution License](https://creativecommons.org/licenses/by/4.0/), which permits use, distribution and reproduction in any medium, provided the original work is properly cited.

used to perform several historical experiments, all using the so-called CMIP6 emission inventories as prescribed by Hoesly et al. (2018) and van Marle et al. (2017). Within these emission inventories we find the aerosol black carbon (BC) and the sulfate aerosol precursor sulfur dioxide which are both produced from fossil fuel burning and biomass burning, and emitted separately from other natural and anthropogenic sources. Together, they represent two crucial components for radiative forcing calculations, with major contributions to both the scattering and absorbing components of aerosol forcing.

A previous study has pointed to the potential errors in the CMIP6 emission inventory for the sulfate precursor sulfur dioxide (Moseid et al., 2020), possibly underestimating East Asian emissions. Emission inventories of aerosol BC as contained in CMIP6 (Hoesly et al., 2018) are associated with medium confidence according to the latest IPCC report (Szopa et al., 2021). In addition, previous studies have suggested historical BC emission can be substantially higher than depicted in current inventories (Bauer et al., 2013; Hodnebrog et al., 2014). Emission trends from the pre-satellite era (before the year 2000 for aerosol parameters) have an unquantified uncertainty and are often a result of scaling of more recent inventory years (Hoesly et al., 2018).

Here, we investigate the concentration of both sulfate and BC in ice as calculated in 11 ESMs used in CMIP6, and compare them with ice core records from 15 cores in nine regions. We analyze the historical era (1850–2014), as we can take advantage of models using the recent best-guess CMIP6 emission inventory and results stored in the CMIP6 database.

Our hypothesis is based on the idea that long-term trends in the concentration of an aerosol species in ice cores are a fingerprint of the aerosol's trend in general atmospheric burden. Therefore, the trends can be used to verify emission evolution over historical times, as compiled in the CMIP6 emission inventory. Assuming models represent the transport and deposition of an aerosol with comparable quality over the historical time span, the calculated concentrations trends should match the concentration evolution recorded in the ice cores with a relatively constant bias over time. An incorrect emission inventory in either sulfate or BC would reveal itself as a bias between the observed and modeled concentration trend in ice for that specific aerosol. Since both sulfate and BC originate from similar source regions in the industrial era, at least on a large scale, the comparison between models and ice cores should show a highly consistent and correlated bias over time for both components.

Using the ensemble of CMIP6 historical model simulations offers the chance to investigate whether such bias is robust across different historical aerosol change reconstructions from a range of ESMs.

The following section will present the ice core and model data, and how the simulated concentrations in ice are calculated. Section 3 will present the results of our analysis, and a subsequent investigation of the potential causes for inter-model differences. Finally, Section 4 discusses how the results match our hypothesis, and Section 5 concludes about the study and what implications it may have.

2. Data and Methods

2.1. Ice Core Data

An overview of the location of the ice cores used in this study is shown in the map in Figure 1. We have selected ice cores where BC and sulfate concentrations were available with at least annual temporal resolution. All are from the Northern Hemisphere with the exception of one. Each ice core is presented individually (see Table 1) except those retrieved from Greenland. These eight ice cores are aggregated and averaged for a Northern and Southern Greenland region, as we found high agreement in BC and sulfate trends across ice cores in these two regions. We note that while we found an ice core site to accurately represent its surrounding area in Greenland, this site-to-area representation may not be extended to other ice core sites due to the large variations in topography. To ensure there is no confusion with other atmospheric “concentration” metrics in use, we define the term “concentration” as being the concentration of an aerosol species (here sulfate and BC) measured in ice cores, when analyzing melted ice cores. The methods for obtaining the aerosol concentrations from the ice cores used here are described in the publications listed in Table 1. Previously unpublished data and methods are described in more detail below.

2.1.1. Sulfate Concentration

Most published sulfate concentration records in ice cores, including the ones we are using here (See Table 1), have been obtained using ion chromatography (IC) detecting the soluble fraction of sulfur in ice (Avak et al., 2019).

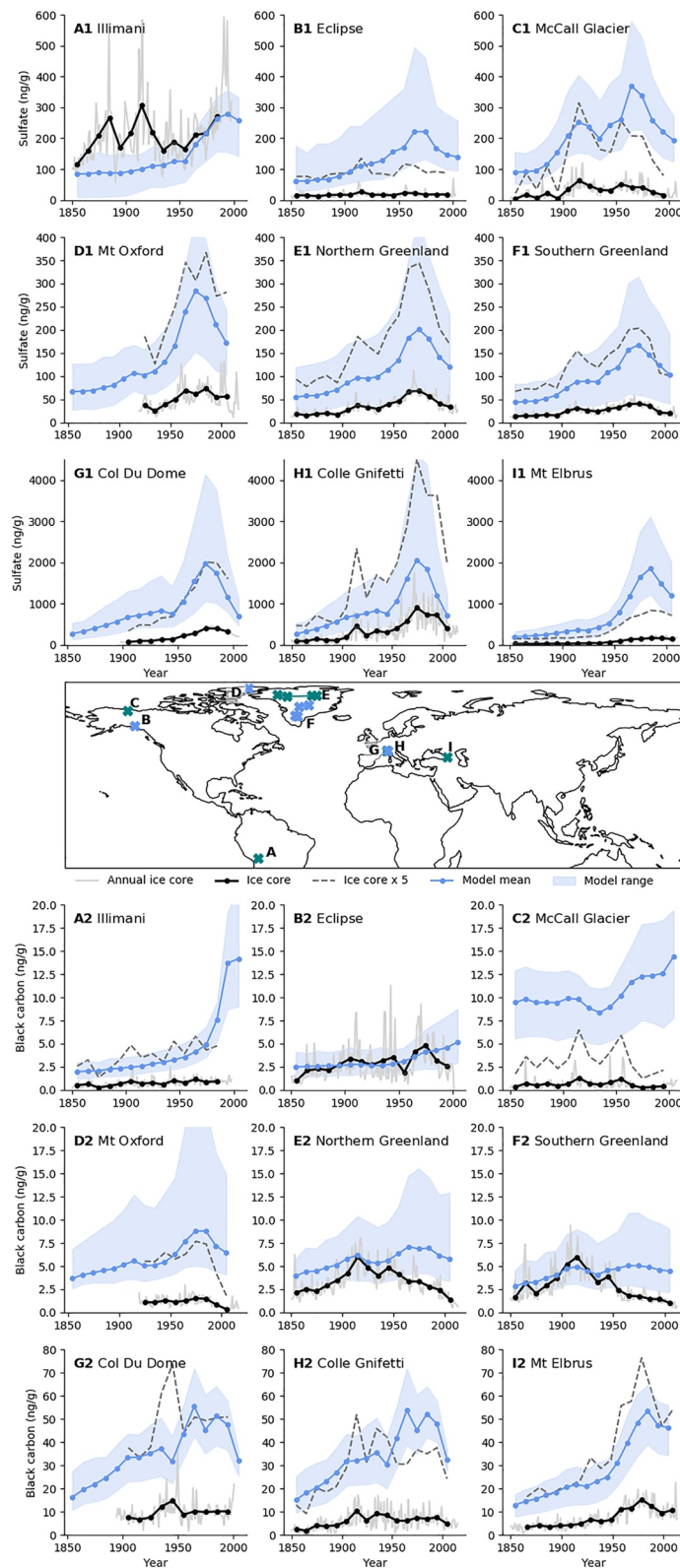


Figure 1. Decadal sulfate (a1–i1) and black carbon (a2–i2) concentrations [ng/g] in ice cores (black) and model mean of 11 models (blue), decadal averaged. The shading shows the maximum/minimum decadal average of the 11 models. The light gray solid line shows the annual ice core concentration. The stippled dark gray line shows the respective decadal ice core concentrations multiplied by a factor of 5.

Table 1
Overview of the Ice Cores Used in This Study Along With Respective References Where Black Carbon and Sulfate Data can be Found

Site	Lat	Lon	BC	sulfate
Illimani	−16.62	−67.76	Osmont et al. (2019)	Kellerhals et al. (2010)
Eclipse	60.5	−139.5	<i>This study</i>	<i>This study</i>
McCall Glacier	69.3	−143.8	<i>This study</i>	<i>This study</i>
Mt Oxford	82.2	−73.2	<i>This study</i>	<i>This study</i>
Greenland				
Northern				
NGT_B19	78.0	−36.4	<i>This study</i>	<i>This study</i>
Tunu2013	78.0	−33.9	http://doi:10.18739/A2ZQ1G	Sigl et al. (2015)
NEEM_2011_S1	77.5	−51.1	Zennaro et al. (2014)	Sigl et al. (2013)
Humboldt	78.5	−56.8	McConnell (2010)	Sigl et al. (2013)
Southern				
Summit2010	72.6	−38.3	http://doi.org/10.18739/A2XV7T	http://doi.org/10.18739/A2XV7T
D4	71.4	−43.9	McConnell (2007)	McConnell (2007)
ACT11d	66.5	−46.3	<i>This study</i>	http://doi.org/10.18739/A2Z933
ACT2	66.0	−45.2	McConnell and Edwards (2008)	McConnell and Edwards (2008)
Col Du Dôme	45.8	6.9	<i>This study</i>	Preunkert et al. (2001) Legrand et al. (2013)
Colle Gnifetti	45.9	7.85	Sigl et al. (2018)	Engardt et al. (2017)
Mt Elbrus	42.4	42.4	Lim et al. (2017)	Preunkert et al. (2019)

Note. Previously unpublished data is referenced as *This study*.

However, the sulfate concentrations in the ice cores newly reported in this study were measured with Inductively Coupled Plasma Mass Spectrometry (ICP-MS). This applies to the Eclipse, McCall Glacier, Mt Oxford, and NGT_B19 ice cores. The ICP-MS method is based on mass spectrometry and has the advantage of detecting all chemical forms of sulfur in the ice. A mix of analysis techniques can lead to discrepancies between measured concentrations of sulfate depending on the technique implemented (IC or ICP-MS). However, in historical times since 1850, the majority of the sulfur in ice cores is soluble sulfate, fully captured during analysis by both IC and ICP-MS. Therefore, the sulfate concentrations are very similar regardless of the technique used to measure them (McConnell et al., 2017). Yalcin and Wake (2001) found that the new ICP-MS-based sulfur measurements in the Eclipse core presented here are in close agreement with earlier IC based sulfate measurements from the same core. Sulfate measured by ICP-MS includes methanesulfonate, which has been shown to account for 3%–5% of the sulfate found in Greenland ice (Legrand et al., 1997). Sulfate can be subject of re-location at ice core sites influenced by meltwater percolation (see e.g., (Eichler et al., 2001)). To avoid such a post-depositional change of the original deposited signal, we chose ice core sites with negligible influence of melting.

2.1.2. Black Carbon

Concentrations of BC in all ice cores were determined with a Single Particle Soot Photometer (SP2, Droplet Measurement Technologies) coupled with a jet or ultrasonic nebulizer to aerosolize the molten ice core samples (McConnell, 2007; Wendl et al., 2014).

Although a number of annually resolved ice core BC (e.g., Liu et al. (2020)) and sulfur (e.g., Sigl et al. (2014)) records spanning this period are available from Antarctica, we chose to focus on ice core record/model comparisons in the Northern Hemisphere and included only one comparison from a tropical site in Southern Hemisphere (Illimani).

Table 2
Altitudes in Meters at Ice Core Sites and in Model Means With Standard Deviation Shown in Parenthesis

Site	Ice Core	Model mean (std)
Illimani	6300	2303 (314)
Eclipse	3017	1031 (185)
McCall Glacier	2400	437 (127)
Mount Oxford	2210	452 (153)
Northern Greenland	2270	2318 (135)
Southern Greenland	3258	2189 (199)
Col Du Dôme	4350	719 (190)
Colle Gnifetti	4452	739 (174)
Mt Elbrus	5115	1001 (194)

Note. Model mean was averaged over 3×3 grid matrix surrounding ice core location and averaged together for the models used. For Northern and Southern Greenland we have used NGT_B19 and Summit2010, respectively.

2.2. Concentrations From ESMs

The Earth system is extremely complex and includes a multitude of interacting processes. As such, several ESMs have been developed with different ways to represent these interwoven processes. To compare these different models and the representations of physical processes within them, the CMIP6 has been initiated as a collaborative effort across the ESM community (Eyring et al., 2016). CMIP6 consists of several model intercomparison projects (MIPs) that design experiments tailored to different aims and focus points; however, here we use only the historical experiment. Every ESM has to perform a set of basic experiments to participate in any of the MIPs of CMIP6. The historical experiment is one of them meant to simulate the climate from 1850 to 2014 and to allow for a comparison to observations and recent climate evolution. Its period was chosen to cover the times where the observational record is comprehensive enough that comparisons and evaluations between the real climate and simulations can be conducted. The historical experiment is forced and driven by a best guess of greenhouse gas concentrations and both natural and anthropogenic aerosol and aerosol precursor emissions.

Here we use the results from 11 of the ESMs that participated in CMIP6. They were chosen based on the availability of diagnostic outputs and variables needed to calculate the simulated concentrations of sulfate and BC at ice core sites in the historical experiment. The sum of dry and wet deposition of sulfate and BC along with total precipitation, co-located with the ice cores, was used to compute concentrations. The ESMs, their horizontal resolution, and corresponding references are listed in Table B2, and further details of the variables used to calculate the concentration of aerosols to compare with ice core data are found in Appendix B1.

2.3. Comparing Ice Core Data to Model Data

Ice cores have been retrieved in topographically varying areas such as on high-alpine mountain glaciers in the European Alps, or in more smooth topographic areas, like on the top of the ice cap of Greenland. In contrast, ESMs represent Earth's surface as a matrix of surface grid cells, at differing horizontal resolutions depending on the ESM (see Table B2). The topographic elevation within each grid cell in a model must represent both the peaks and the valleys within the area it covers. This means that the topography in each grid cell is a flat surface at the average altitude of the grid cell. Therefore, a point measurement such as an ice core taken at any location of a high mountain peak, will correspond to an ESM grid cell at a lower elevation, as shown in Table 2. Especially in mountain areas, we can expect the ESM to exhibit higher concentrations than measured at the ice core site due to the representation error. However, this bias is probably not changing much over historical time scales, and we assume that trends in models and in ice cores are expected to be correlated.

As we are interested in the long term trends of aerosol concentration and less so in a model's ability to represent local meteorological conditions, and since models show variability in deposition between close-by grid cells, we further extend the area from which model data are taken for the comparison of aerosol concentrations at the ice core site. In particular, we use the nearest neighbor method to find the grid cell closest to the ice core location, and then find the surrounding 3×3 grid cells and average them with equal weight.

ESMs do not output aerosol concentration in snow and ice directly, therefore it is calculated here based on the wet and dry deposition of the aerosol and total precipitation in the chosen area:

$$conc = \frac{\sum_1^9(wet + dry)}{\sum_1^9 prec_{ice+liq}} \quad (1)$$

where *conc* is the concentration of the aerosol component in question, and wet and dry refers to the sum of deposition of the aerosol in the nine grid cells, divided by the total ice and liquid precipitation prec in the same nine grid cells. Aerosol concentrations as calculated from the models and as measured in the ice cores are then

averaged over 10 year intervals, starting at the beginning of each decade. Altogether, this is done to compare the long-term trends in aerosol concentration rather than the inter-annual variability in the data, which would be primarily due to changes in meteorological conditions. As detailed in Legrand et al. (2018), the dating error of an ice core typically ranges from 1 year in the upper layers to 5 years prior to 1930 along the 1890–2000 AD ice-record extracted at the Col Du Dôme site, so dating errors in ice cores would not impose biases to the decadal averaged data as shown in this paper.

While the concentration is straightforward to calculate, there is no way to determine the source regions of the aerosols at ice core sites in the CMIP6 simulations. Additional simulations are therefore conducted with one of them, the ESM NorESM2-LM, as described in the following section.

2.4. Emission Experiments With NorESM2-LM

To investigate which emission source areas affect aerosol concentration in the ice core locations, we have designed seven perturbation experiments and one control experiment. In a first set of experiments, the anthropogenic emissions of either BC or sulfur dioxide (aerosol precursor of sulfate) each are doubled in one of three regions at a time. The regions are defined according to the HTAP2 definitions as described in Galmarini et al. (2017) and represent Europe, Asia, and North America. This adds up to six experiments, and in a seventh experiment, the emissions from global wildfires were doubled (BC, sulfate, and organic matter), to investigate to what extent natural and anthropogenic biomass burning contribute to concentrations of BC and sulfate. An overview of experiments is found in Table A1. To reduce inter-annual variability through forcing and feedback on the circulation and tracer transport in these perturbation experiments, the sea surface temperatures (SSTs) and sea-ice cover (SIC) were fixed to the SSTs and SIC fields extracted from the NorESM2-LM fully coupled historical experiment. We also performed one control experiment with unmodified emissions as in the historical simulation, using the same prescribed SSTs and SICs. In all of the experiments the aerosol emissions are based on the CMIP6 anthropogenic (Hoesly et al., 2018) and biomass-burning (van Marle et al., 2017) emission inventories. The experiment names and descriptions including the varying emission perturbations are presented in Appendix A.

The aerosol concentrations at different ice core locations from these experiments are then used to calculate and estimate regional contributions. For this calculation we assume linearity, meaning that a doubling of emissions is expected to double the concentration. In order to assess the contribution of aerosols from each source region or wildfire, the aerosol concentration in the control simulation (histSST in Table A1) is simply subtracted from each of the individual experiments. The remainder is then the aerosol concentration believed to stem from the particular source region (or wildfire emissions) tested in the experiment.

3. Results

3.1. Sulfate and BC in Ice Cores and Models

Figure 1 compares the simulated concentration of sulfate (a1–i1) and BC, a2–i2 with the measured concentrations from seven ice cores and two composites from ice core in northern and southern Greenland. It displays the decadal average from the 11 models used in this study (blue solid line) and the model spread defined as the minimum and maximum decadal model average (shaded blue). The ice core concentrations (black solid line) are based on one ice core, except for the two areas Northern Greenland and Southern Greenland which are based on several ice cores (see map in Figure 1 and Table 1).

The model means of the sulfate concentrations show a general increase until the mid-to late 1970s across Northern Hemisphere ice core areas, followed by a subsequent significant decrease in concentration. The model spread in decadal sulfate concentration is large across regions, especially in the decades before and after the 1970s. We find that the models in general show a sulfate concentration larger in magnitude than what is recorded by the ice cores. The models with the lowest concentrations are very close to the measured sulfate, in particular in Greenland and Colle Gnifetti. However, one can still identify a similar temporal evolution in ice core and models for sites such as Mt Oxford, Northern and Southern Greenland, Col Du Dôme, Colle Gnifetti, and, to some extent, Mt Elbrus. We also added a gray stippled line in Figure 1 showing five fold the decadal ice core observation data in areas where the ice core data is outside the range of the models, which is every area except Illimani for sulfate. We refer to this graph as the five factor ice core data, and it helps visually to compare magnitude and

trends between models and ice cores. For example, we see that both model means and ice core concentrations of sulfate show similar temporal trends with two maxima in the area surrounding McCall Glacier. However, there is a model-observation discrepancy as to when the two temporal maxima are largest in magnitude. The five factor lines also illustrate that the model mean concentration of sulfate in Col Du Dôme is approximately a factor of five higher than the ice core data, while in Northern and Southern Greenland the model mean concentration is higher by a factor of three to four.

The five factor ice data shows the ice core trends more clearly, and highlights that models in general are able to reproduce the evolution of sulfate concentrations, while they are unable to reproduce their magnitude. There may be several reasons the overestimation of the sulfate concentrations by the models. Recall from Section 2.3, all models are unable to resolve the real surface topography, meaning that the elevation in the ice core sites are not represented in the models (Table 2), explained as representation error above. Second, as we use a 3×3 grid box area surrounding the model grid cell closest to the ice core location (as explained in Section 2.3), grid boxes that are closer to aerosol emission sources than the actual ice core site are included in the model average, giving a larger absolute concentration value. This is especially relevant for ice cores close to sources such as Col Du Dôme and Colle Gnifetti in the European Alps. We note that when performing the same analysis with a 1×1 grid box area we see trend-wise the same results as with a 3×3 grid. However, even if their magnitude differs, the sulfate comparison shows that the trends are well correlated, indicating consistency between the temporal evolution of sulfur emissions and sulfate concentrations in ice core archives.

In general, the absolute magnitude of BC concentrations is much lower than that of sulfate (see Figure 1a2–1i2). The temporal evolution of BC concentrations differs more prominently between ice cores and models than what was shown above for sulfate. Only at Mt Elbrus and, to some extent, Mt Oxford, comparable temporal trends appear between model and ice core data throughout the analyzed time period. Modeled BC concentration at Illimani shows a sharp increase in the most recent period which is not measured in the ice core. We also find that while the model mean concentration of BC has maximum values post-1950 in the European Alps, the ice core data show a pre-1950 maximum of BC concentration in both sites (Col Du Dôme and Colle Gnifetti).

In fact the maximum in modeled BC concentration occurs after 1950 for all sites. However, at five out of nine areas, the maximum in the ice core data occurs before 1950. Also in both Greenland areas the comparison shows a clear discrepancy between the model data, with present-day ice core BC concentrations lower than pre-industrial values, and a distinct maximum in the early 1900s.

Another feature to note from the comparison is the inter-model range in BC concentrations in the European Alps, McCall Glacier and Mt Elbrus, which stays close to constant over time (Figures 1g2, 1h2, 1c2, and 1i2), as opposed to other areas like Illimani, Eclipse, Mt Oxford and both regions of Greenland where the inter-model range increases with time (Figure 1a2, 1b2, 1d2, 1e2, and 1f2). A constant model range indicates high model agreement in concentrations, while a diverging model range indicates that inter-model differences become more important with time. In the following we investigate two representative ice core sites, Colle Gnifetti and Northern Greenland, more closely, because they represent this difference in the evolution of the inter-model range of BC concentrations.

3.2. Inter-model Differences at the European Alps and Northern Greenland

We find the largest model range at Colle Gnifetti (European Alps) for sulfate concentrations in the 1970s and –80s (Figure 1h1). In Figure 2a we can find the ESMs that are responsible for this range. Models with maximum sulfate concentration in the high emission era are MIROC6, MPI-ESM-1-2-HAM and MRI-ESM2-0. These models have at the same time widely varying pre-industrial background sulfate concentrations. To further investigate inter-model trend differences we present the data as a percent change from their respective pre-industrial values of the period 1850–1865 (Figure 2b). The ice core observations show a maximum increase of 800% from pre-industrial values, which is in the middle of the model range of 400%–1200% change. The long-term relative trend in sulfate concentration at Colle Gnifetti is well represented in all models of this study.

Figures 2c and 2d show BC concentration at Colle Gnifetti in absolute values and percentage change from the pre-industrial era, respectively. Identical to Figure 1h2, in general the absolute model concentrations are higher than ice core values.

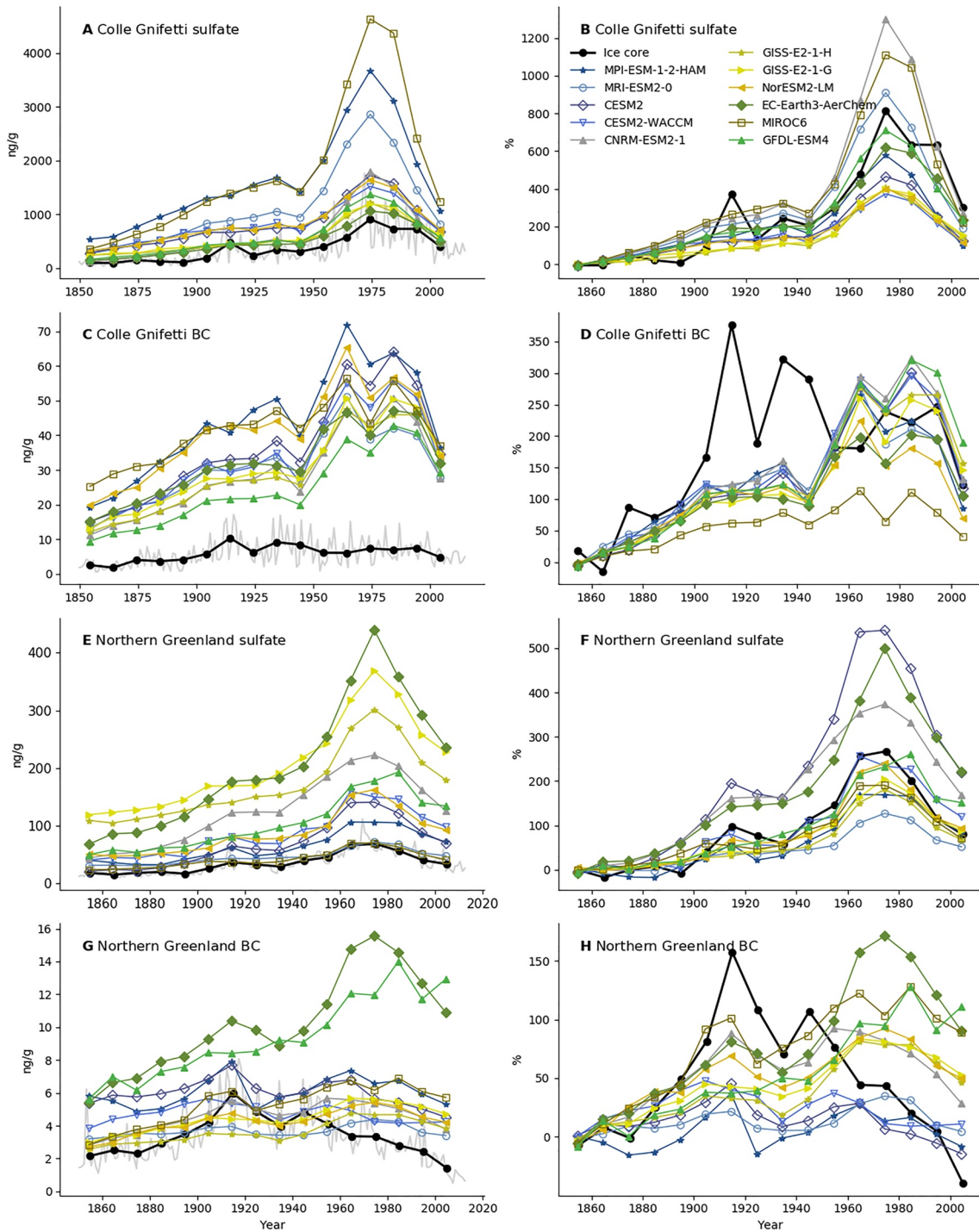


Figure 2. Concentrations of sulfate and black carbon in absolute values (left column) and percent change from pre-industrial (right column) for Colle Gnifetti (a–d) and Northern Greenland (e–h). Percent change is calculated using the first 15 years of each respective timeseries as baseline.

Note also that there are evidently inter-model differences in pre-industrial concentration values. The percentage changes from pre-industrial values (Figure 2d) clearly show a maximum BC concentration recorded in the ice core in the early 20th century, while all models agree on a late 20th century maximum. This was also apparent in the five factor ice core data shown in Figure 1h2.

Figures 2e–2h show absolute and percentage change in sulfate and BC concentrations according to the 11 models of this study together with the respective averages of four ice cores located in Northern Greenland (see Table 1).

For the sulfate concentration, some models have comparable values to that of the ice cores, while others grossly overestimate the absolute concentrations. We note that the model with the highest concentration value is EC-Earth3-AerChem, which is the model with the lowest sulfate concentration at Colle Gnifetti (Figure 2a). Likewise, similar opposite findings are found for MIROC6, which was the model with the highest sulfate concentrations at Colle Gnifetti, but has the lowest values in Northern Greenland. EC-Earth3-AerChem is the model of this study with the highest global lifetime for sulfate (6.7 days in the present day, see Figure C1), and MIROC6 is the model with the lowest global sulfate lifetime (2 days in the present day, see Figure C1), as computed from global burden and deposition. A long lifetime means that a particle is transported longer before being deposited. For these two models, global lifetimes explain why a model depositing in large magnitudes close to emission sources (i.e., Colle Gnifetti) does not deposit as much in a pristine remote area (i.e., Northern Greenland) and vice versa. However, for the rest of the models global lifetimes (see Figure C1) do not explain so straightforwardly the order in sulfate concentration differences between Europe and Northern Greenland as shown in Figures 2a and 2e. The graph showing percent change of sulfate concentration illustrates that the recorded changes from ice cores in Northern Greenland are in the middle of the model range. The relative sulfate concentration trends in Northern Greenland are well represented by all of the models in this study (Figure 2f).

The absolute values of BC concentrations in Northern Greenland differ largely between models and ice core data. According to the ice core records there is a maximum of BC concentrations in the early 20th century, followed by a continuous negative trend after 1950 (Figure 2g). The models do not represent this evolution, which is clearly shown in both Figures 2g and 2h. EC-Earth3-AerChem and GFDL-ESM4 have the largest BC concentrations in the end of the 20th century of about 15 ng/g (Figure 2g), but when looking at the percentage change, multiple models have an overall positive trend since pre-industrial times. The models disagree not only with the ice core records, but also among each other regarding the long-term BC concentration trends in Northern Greenland. The differences in timing of BC concentration maxima are significant, and the source region of the BC arriving at the different ice core sites is of interest. An investigation using source region attribution within only one model has been thus added to this study.

3.3. Emission Region Attribution Using NorESM2-LM Experiments

Concentration contributions from different source regions of both sulfate and BC at all ice core areas of this study have been calculated as explained in Section 2.4, and the result is shown in Figures 3 and 4, respectively.

For most of our ice core areas the sum of sulfate contributions (bars in Figure 3) does not add up to that of the reference simulation (dark green), which means that other sources than those we chose in our perturbation experiments contribute to the total sulfate concentration. Other sources comprise natural emissions of DMS and SO₂ from volcanic activity, as well as anthropogenic emissions from other regions of the world.

In fact, most of the sulfate concentration in Illimani can be attributed to other source areas (such as Southern America), while for Eclipse, McCall Glacier, and Mt Elbrus other sources account for about half of the simulated total sulfate concentration. North American sulfur dioxide emissions dominate among our selected perturbation sources in Eclipse, McCall Glacier and both Greenland areas, and one can note increasing Asian contributions in the end of our investigated period. Unsurprisingly, almost all sulfate found in Col Du Dôme and Colle Gnifetti can be attributed to European emissions according to NorESM2-LM. Biomass burning is not a large contributor to sulfate concentrations in any of the ice core sites, but acts as the definite main contributor to BC concentrations at Illimani (Figure 4a).

Biomass burning is an important contributor to BC concentrations through the investigated period for all ice core areas except for the European Alps. The most diverse contribution sources of BC concentration is found in Mt Oxford and both Greenland areas. For example, in Southern Greenland in 1970–1980, all four contributors account for 20%–33% of the total BC concentration in NorESM2-LM. Almost all of the simulated BC concentration at Col Du Dôme and Colle Gnifetti can be attributed to European anthropogenic emissions of BC, but more interestingly European emissions also dominate among the contributions in Northern Greenland. Between 1900

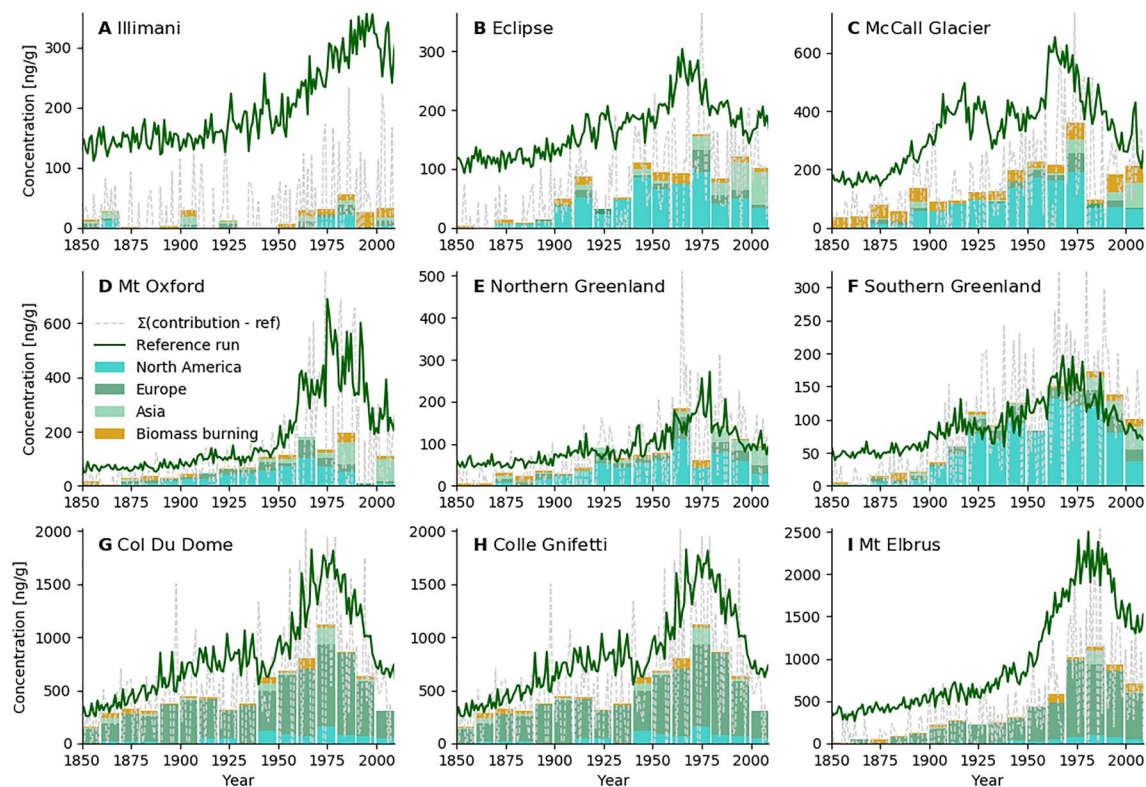


Figure 3. Decadal contributions of sulfate from three emission source regions and biomass burning according to NorESM2-LM. The dark green line represents the reference simulation, and the gray stippled line shows the sum of error for the contribution experiments.

and 1990 European contributions account for 20%–57% of the total BC concentration there (Figure 4e). Asian emissions of BC become more prevalent in the last decades at many ice core sites, but especially at Eclipse.

Recall that NorESM2-LM contributions in theory are decompositions of the control simulation result, and as the previous Section showed, this control simulation does not accurately represent the BC concentration as recorded in ice cores in Northern Greenland and at Colle Gnifetti (Figures 2d and 2h). Therefore, the contribution bars shown in Figures 4e and 4h are a visualization of the components that add up to a biased evolution in BC concentration.

4. Discussion

4.1. Sulfate Concentrations

The relative trend of sulfate concentrations from ice core records over the industrial era agree with that of the 11 ESMs in this study in 7 out of 9 regions. We find inter-model agreement in sulfate concentration trends thus almost independent of ice core location, although there is disagreement between models regarding absolute magnitudes of concentration. This indicates that generally CMIP6 emission inventories represent historical trends in the sulfate precursor sulfur dioxide well. Anthropogenic sulfur dioxide emissions in Europe were at their maximum during the 1970s and –80s according to CMIP6 emission inventories (Figure A1 and Hoesly et al. (2018)), which is also when we find the largest model range.

By applying the NorESM2-LM models for source attributions, we found European SO₂ emissions as major sulfate sources for the European ice core sites, whereas North American sources dominate at Greenland sites. Fagerli et al. (2007) assessed contribution regions for sulfate deposition rates at Col Du Dôme and Colle Gnifetti using the EMEP model. They also concluded that the main contributor to sulfate found on Colle Gnifetti and Col Du Dome were European emission sources. Engardt et al. (2017) investigated sulfur concentration in Europe in the 20th century using two chemical transport models (EMEP MSC-W and MATCH) and ice core records from Colle Gnifetti. They found that both models represented non sea salt (nss) sulfate concentration trends well,

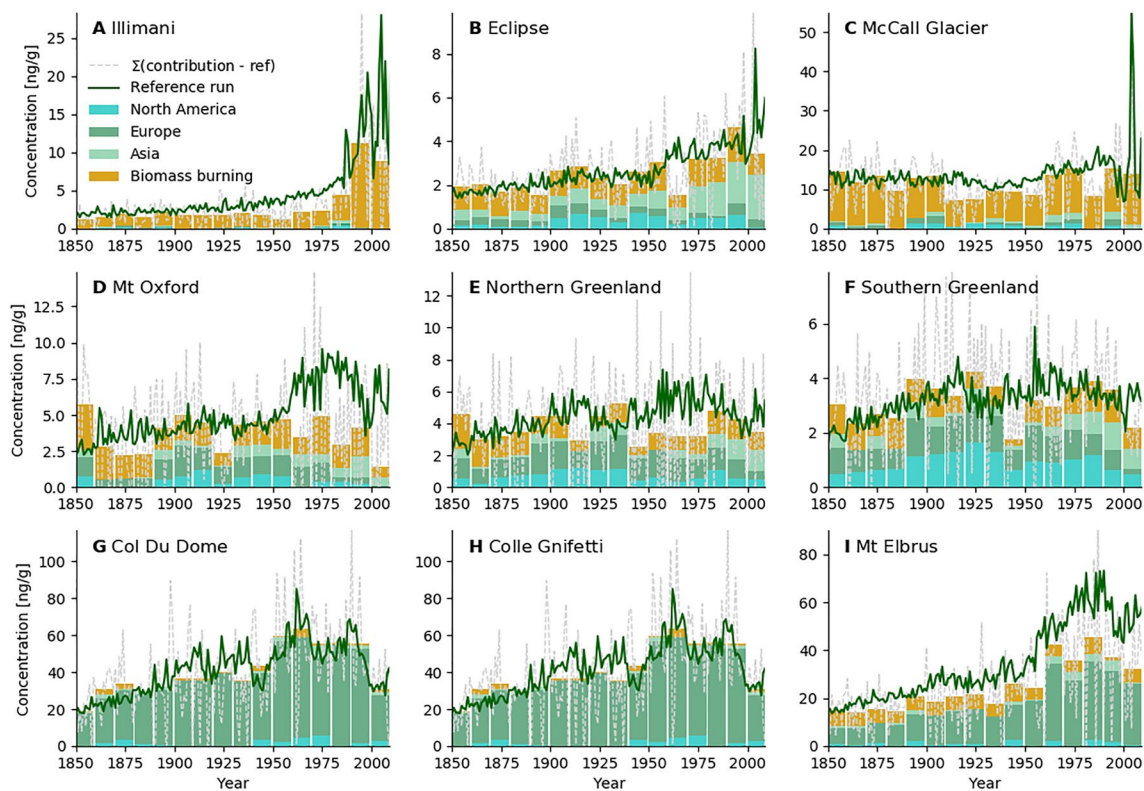


Figure 4. Decadal contributions of BC from three emission source regions and biomass burning. The dark green line represents the reference simulation, and the gray stippled line shows the sum of error for the contribution experiments.

comparable to Fagerli et al. (2007), Bauer et al. (2013), and this study. The maximum nss-sulfate concentration in EMEP MSC-W and MATCH at Colle Gnifetti was larger than the ice core recorded maximum nss-sulfate concentration by a factor of three and nine, respectively. We incorporated two NASA-GISS models in this study, and a previous generation of the atmospheric model (GISS-modelE) has been used to compare model to ice core records in Bauer et al. (2013). Three Greenland ice core sulfate records (Humboldt, D4, and ACT2, also used in the current study, see Table 1) from Bauer et al. (2013) agree well in trend with that using all the different setups of the GISS modelE using CMIP5 emissions (Lamarque et al., 2010). Together with the results of this study we suggest both CMIP5 and CMIP6 emission inventories of the aerosol precursor sulfur dioxide do capture overall emission trends in the Northern Hemisphere with a maximum in the 1970s and a decline since then. The ice core data available provide little constraint and verification for the East Asian sulfur emissions, since East Asian sources contribute only a small part to the sulfate recorded in the ice core archives (Figure 3).

There exist few previous multimodel studies evaluating sulfate concentrations using ice cores; all have found that although agreeing in trend, the models disagree in magnitude. The difference in concentration magnitude between models and ice cores is suggested to be in part a result of the lower elevation in grid cells in the model, and this rationale holds for all mountain sites apart from Greenland and possibly Illimani. Due to a closer proximity to emission sources, sulfate concentrations are higher at lower altitudes. Furthermore, the high-alpine glaciers are often in the free troposphere where aerosol concentrations in air are low (especially during cold season) (Engardt et al., 2017).

However, this representation error does not explain the bias at all ice core sites in the current study, as models represent high altitudes for Greenland sites, while still overestimating the sulfate concentration there. Even pre-industrial sulfate concentrations are overestimated in most models in Greenland. Note, however, that the model with the lowest concentration traces the evolution of the Greenland data quite well. The comparison at the Greenland sites suggests that the transport from anthropogenic sources in the Northern Hemisphere to these remote ice cap sites in Greenland is too efficient in most models.

The Illimani is the only site where ice core sulfate concentrations exceeds model estimates. The large variation in the observed record, the small increase after 1950, as well as the location on the western edge of South America suggest that other sources than fossil fuel burning are responsible for most of the sulfate found here. Diffuse volcanic and marine sulfur sources are incorporated in some models, but the comparison suggests that other sources, such as sulfur from for example, explosive eruptions or from mining activities may play a role.

4.2. Black Carbon Concentrations

Trends in BC concentrations agree between decadal model mean and ice core records at Mt Elbrus, and to some extent Mt Oxford throughout the analyzed period. The two ice core records from the European Alps show a pre-1950 maximum in BC concentration, while all models agree on a post-1950 maximum in this area. In both Greenland areas, however, the models disagree between each other in BC concentration trends in addition to a bias in the ice core data.

As discussed above, the sulfate concentration trends are rather well represented by the simulations, and the models of this study perform well regarding formation, transport and deposition of sulfate. When models perform well in transport of one aerosol component they should perform well for another aerosol component, as transport within a model is a priori and not aerosol component dependent. However, emission amount, source regions and timing as well as processes leading to deposition are dependent on aerosol components. Thus, the apparently different temporal evolution of BC concentrations in ice core data and models can likely be due to discrepancies in either the CMIP6 BC emission inventory, or specific model deposition processes, or a combination of the two. As there is high inter-model agreement in the biased timing of the BC concentration maximum in the European Alps, we suggest errors in BC emission inventories is the source of this bias between models and observations. For Greenland this is slightly different. When multiple models are given the same input emission inventory, and we assume overall transport is correct, inter-model discrepancies in trends in BC concentrations point to inter-model deposition process differences. Inter-model deposition comparisons are outside the scope of this paper, but a thorough investigation of deposition schemes and the effect this has on BC dry and wet deposition in the CMIP5 ensemble can be found in Allen and Landuyt (2014), which also found a large range in modeled BC deposition across models. Deposition process differences could reflect distinct parameterisations for a BC particle to become hydrophilic by coating of solubles. These will cause inter-model differences in BC lifetime, varying differently over time (See Figure C2; Bond et al. (2013)). However none of the models, despite their differences in BC lifetime, represent the ice core recorded temporal evolution of BC concentration, and we suggest that the source of error in Northern and Southern Greenland is a combination of errors in emissions and differences in model deposition processes.

A yet to be discussed potential cause of bias is the effect of circulation changes caused by the self-lifting of absorbing aerosols. Previous studies have investigated this non-linear effect for biomass burning events (Boers et al., 2010; de Laat et al., 2012; Ohneiser et al., 2021), however limited studies exist on the potential magnitude of this bias regarding anthropogenic emissions, and we make no attempt to estimate the magnitude of such a bias in the current study. In addition, models may differ in their approach for injecting emissions from biomass burning, where different injection heights would affect transportation. However, such an intermodel difference would not evolve over time and can be assumed to be a constant source of bias throughout the investigated time period, and is therefore not given attention in the current analysis of aerosol long-term trends.

We investigated which emission source region contributed to the NorESM2-LM BC concentration in Northern Greenland and found that a large amount came from European sources. North American BC emissions have been thought to be a main contributor to BC in Greenland (Bauer et al., 2013) but on average in NorESM2-LM North America accounts only for 17% of the total concentration in the northern part, and 28% in the southern part of Greenland.

Almost all of the BC at Colle Gnifetti and Col Du Dôme originates in Europe; this again points to wrong European emission data as possible reason for the bias between NorESM2-LM and the ice core data of these two sites. Since European emissions contribute to BC concentrations in Northern Greenland as well, at least part of the Northern Greenland bias for NorESM2-LM can be related to erroneous CMIP6 emission inventories of European anthropogenic BC.

Bauer et al. (2013) assessed the reconstruction of historical BC evolution between GISS-modelE and three Greenland ice cores, and found an early 20th century peak in the Greenland ice cores that is not present in the model data. This is what we found in Figures 2g and 2h. Bauer et al. (2013) suggest a missing source in emission inventories may be the cause of this bias, which supports our findings. While several ice core sites exhibit considerable representation errors for sulfate, Greenland and Eclipse are an exception. The bias of the model mean and ice core data between 1900 and 1950 is relatively small, although sulfate at the same time is underestimated by a factor of 3. This is another argument for a possible underestimation of BC emissions in this part of the century.

The differences in model range evolution in Figure 1a2–i2 may be a result of inter-model differences in BC lifetimes. At some ice core sites the inter-model range is changing over time, while at others it stays rather constant. When investigating the sources for BC in nine ice core areas, according to NorESM2-LM (Figure 4), we find that the areas with a close to constant model range (see McCall Glacier, Col Du Dome, Colle Gnifetti and Mt Elbrus in Figure 1) are relatively close to their emission sources. At sites where the emission sources are far away it seems that differences in BC life time enhance the inter-model range in periods with higher emissions.

At McCall Glacier, almost all BC concentration can be sourced to biomass burning in NorESM2-LM (e.g., boreal wild fires in Northern Canada and Siberia) and the model range in Figure 1c2 stays near constant for this area. For sulfate our results suggest that the models have problems simulating the low concentrations at this Arctic high elevation site. In contrast, the nearby ice core site Eclipse has a diverging model range (Figure 1b2) while simultaneously as contributions from far-away sources such as Asia increase, according to NorESM2-LM. The absolute bias between models and data is small at this site, a location with larger exposure to inflow from the Pacific. The inter-model spread becomes larger in the area surrounding Eclipse as the far-away emission sources in Asia become more important in the last decades (Figure 4). For the last decades the models simulate an increase in BC concentrations, consistent with an increase in Asian emissions. This is however not found in the ice core data at the Eclipse site, possibly because wildfire sources and their variability are dominating the ice core signal.

5. Conclusion

We have gathered sulfate and BC data from 15 ice cores in nine regions and compared their concentrations to those calculated using 11 ESMs, which have participated in the recent CMIP6 exercise. The ice core data have been carefully compiled to provide a benchmark to test inter-decadal concentration evolution of BC and sulfate in a consistent manner. By investigating both components at the same time a more consistent picture of emissions and their evolution can be obtained.

Concentration trends as recorded in the ice cores agree with each other across large regions for sulfate, and this evolution is also captured in the modeled sulfate concentration trends. Both modeled and observed sulfate trend largely correlate to trends in global emissions of the sulfate precursor sulfur dioxide. We can conclude that the emission changes of sulfate precursors in the CMIP6 emission inventories are consistent with the observations presented here. East Asian emissions cannot be tested as rigorously because the location of the ice cores is not ideal to track them.

BC concentration trends vary across ice core sites, but observations from the European Alps and Greenland agree on a distinctive early 20th century maximum which is not present in the modeled BC concentration. In the European Alps there is high inter-model agreement on a bias in timing of the maximum BC concentration. Based on this we suggest CMIP6 emissions for BC in Europe are likely underestimated in the first half of the 20th century.

Errors in BC emission inventories have implications for all future and past studies where CMIP6 historical simulations are compared to observations relevant to aerosol forcing. This includes studies evaluating historical surface temperature, energy balance at the surface and top of atmosphere, ice nucleating particles, and historical cloud studies, to name a few.

European emissions contribute significantly to BC concentrations in 6 out of the 9 regions in this study according to NorESM2-LM, and erroneous input data likely contribute to the ice core-model bias in these regions. Emission region attribution studies with models other than NorESM2-LM would benefit the analysis of far-from-source ice core sites to further narrow the potential source of bias, together with a further investigation of BC deposition processes in ESMs.

Appendix A: Contributions According to NorESM2-LM

Figure A1 shows global emission rates of SO₂ and BC in NorESM2-LM (black solid line), together with the contribution from anthropogenic activity in our chosen areas and from biomass burning globally. The sum of the contributions do not add up to the global emission rate, and this sheds light on how much of the global emission rate can be attributed to both natural and anthropogenic sources from the rest of the world, including shipping and volcanic contributions (see Table A1).

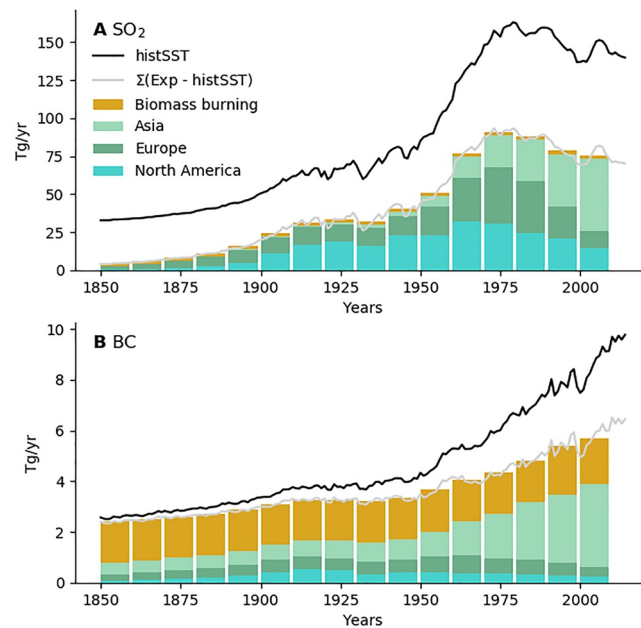


Figure A1. Emissions of SO₂ (top) and BC (bottom) as a function of time. The black line shows global emissions from the reference simulation (histSST in Table A1), the bars show decadal mean contribution per perturbation experiment together with the annual sum of error for the four contributions in gray.

Table A1

Emissions for CMIP6 Are Described in Hoesly et al. (2018) for Anthropogenic Emissions and in van Marle et al. (2017) for Biomass Burning Emissions

Experiment	Emission perturbation				Ocean model
	Species	Region	Sector	Size	
historical	–	–	–	–	Full ocean
histSST	–	–	–	–	SST/SIC prescribed from historical
histSST-so2x2nam	SO ₂	North-America	Anthrop.	+100%	SST/SIC prescribed from historical
histSST-so2x2eur	SO ₂	Europe	Anthrop.	+100%	SST/SIC prescribed from historical
histSST-so2x2asi	SO ₂	Asia	Anthrop.	+100%	SST/SIC prescribed from historical
histSST-bcx2nam	BC	North-America	Anthrop.	+100%	SST/SIC prescribed from historical
histSST-bcx2eur	BC	Europe	Anthrop.	+100%	SST/SIC prescribed from historical
histSST-bcx2asi	BC	Asia	Anthrop.	+100%	SST/SIC prescribed from historical
histSST-biox2	SO ₂ , BC, OM	Global	Biom. burn.	+100%	SST/SIC prescribed from historical

Note. Asia refers to South Asia + Eastern Asia + Central Asia (excluding Russia, Southeast Asia and Middle East). SST/SIC : prescribed sea surface temperature and sea-ice cover. The experiment for biomass burning includes the species for Organic Matter (OM), as this specie indeed is emitted through biomass burning in addition to interacting with BC in NorESM2-LM.

Appendix B: Inter-Model Differences in Ice Core Areas

Table B1
Altitudes in Meters Averaged Over 3 × 3 Grid Matrix Surrounding Ice Core Location in the Models Used

Location	A	B	C	D	E	F	G	H	I
Abbreviation	ILI	ECL	MCC	MTO	NGR	SGR	CDD	CGN	MTE
Ice Core	6300	3017	2400	2210	2270	3258	4350	4452	5115
NorESM2-LM	1854	656	403	376	2087	1746	550	550	811
GISS-E2-1-H	2264	949	161	187	2178	2164	471	548	844
GISS-E2-1-G	2460	966	442	535	2170	2094	532	634	740
EC-Earth3-AerChem	2084	924	393	454	2206	1922	547	547	738
MPI-ESM1-2-HAM	2068	939	339	218	2463	2237	674	674	1220
CESM2	2505	1238	584	562	2434	2338	922	922	1208
CESM2-WACCM	2508	1242	581	550	2426	2328	930	930	1211
GFDL-ESM4	3001	1267	589	586	2292	2316	1032	1032	1002
CNRM-ESM2-1	2282	1161	506	679	2424	2343	841	857	1021
MRI-ESM2-0	2007	933	387	439	2391	2382	658	658	1213
MIROC6	2300	1066	424	384	2428	2213	755	784	999

Note. Letters refer to locations as listed in Table 1. For Northern and Southern Greenland we have used NGT_B19 and Summit2010, respectively. ILI: Illimani, ECL: Eclipse, MCC: McCall Glacier, MTO: Mount Oxford, NGR: Northern Greenland, SGR: Southern Greenland, CDD: Col du Dome, CGN: Colle Gnifetti, MTE: Mt Elbrus.

B1. Model Data Downloaded From ESGF

Tables B1 and B2 shows an overview of the 11 models used in this study. For the historical simulations one ensemble member per model was downloaded, with the variant label r1i1p1f2 for CNRM-ESM2-1, r3i1p1f1 for MPI-ESM1-2-HAM, r1i1p3f1 for both GISS-models and r1i1p1f1 for the rest. The variables downloaded were pr, wetbc, drybc, wetso4, dryso4, emiso2, emibc, mmrso2, mmrbc, mmrso4, airmass, and areacella per model. The models EC-Earth3-AerChem, MPI-ESM1-2-HAM, CNRM-ESM2-1, and both GISS models did not have the variable “airmass” available, we then calculated airmass by using the pressure at each vertical layer together with the Python package `geonum.atmosphere` (Figures B1 and B2).

Table B2
Earth System Models Used in This Study

Institution	Model	Resolution	Reference	Aerosol scheme
NCAR	CESM2	1.25 × 0.9	Danabasoglu et al. (2020)	MAM4
NCAR	CESM2-WACCM	1.25 × 0.9	Danabasoglu et al. (2020)	MAM4
CNRM-CERFACS	CNRM-ESM2-1	1.4 × 1.4	Séférian et al. (2019)	TACTIC_v2
HAMMOZ-Consortium	MPI-ESM1-2-HAM	1.876 × 1.875	Tegen et al. (2019) Mauritsen et al. (2019)	Based on M7
EC-Earth-Consortium	EC-Earth3-AerChem	3.0 × 2.0	van Noije et al. (2021)	Tracer Model v5
NOAA-GFDL	GFDL-ESM4	1.25 × 1.0	Dunne et al. (2020)	Bulk aerosols
NCC	NorESM2-LM	2.5 × 1.875	Seland et al. (2020)	OsloAero5.3
MRI	MRI-ESM2-0	1.125 × 1.125	Yukimoto et al. (2019)	MASINGAR mk-2r4c
MIROC	MIROC6	1.4 × 1.4	Tatebe et al. (2019)	SPRINTARS
NASA-GISS	GISS-E2-1-G	2.5 × 2.0	Kelley et al. (2020)	MATRIX
NASA-GISS	GISS-E2-1-H	2.5 × 2.0	Kelley et al. (2020)	MATRIX

Note. More information about the different aerosol schemes can be found within the references listed in the table.

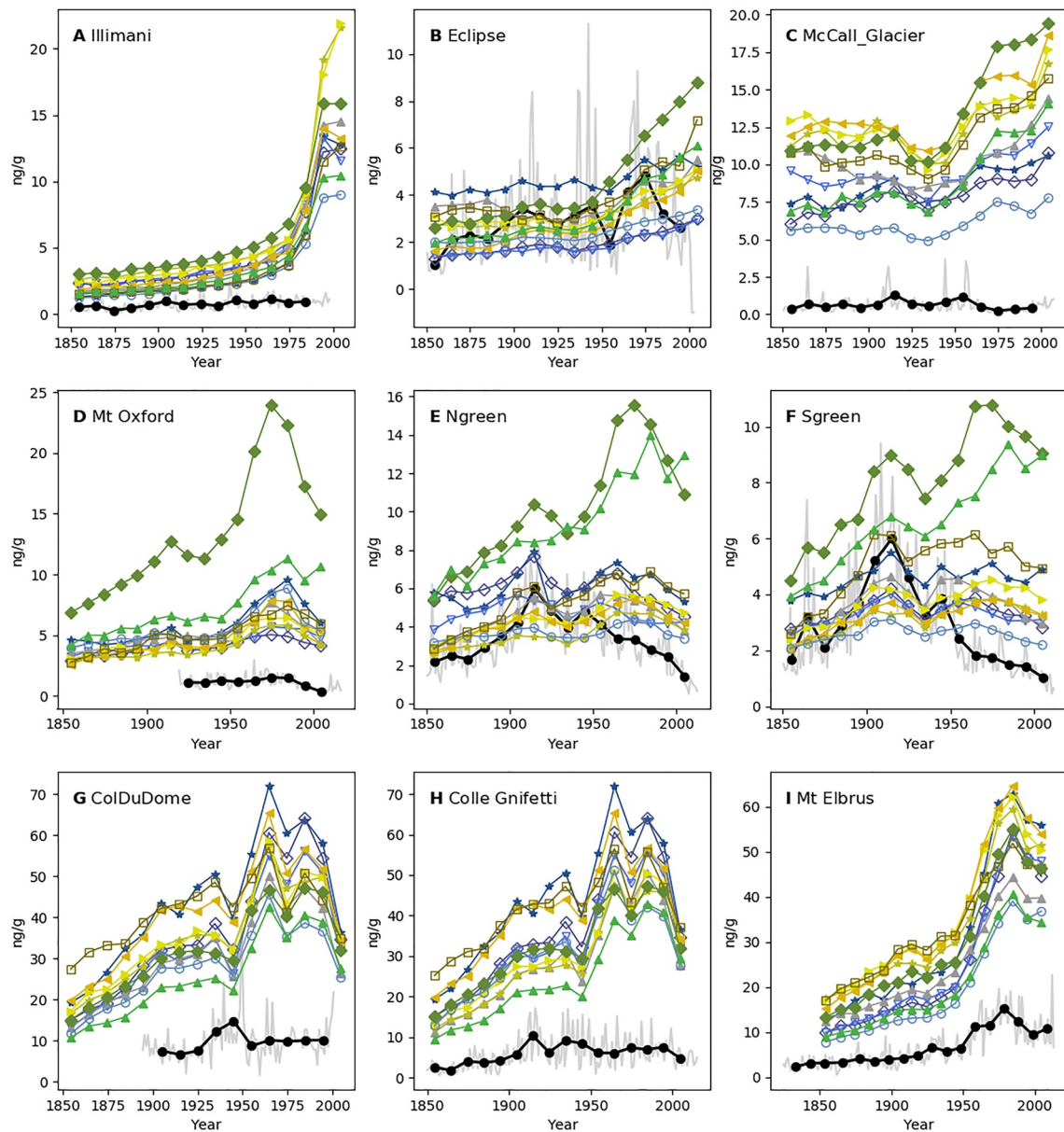


Figure B1. BC concentrations for the ice core sites shown in Figure 1 per model. The legend can be seen in Figure C2.

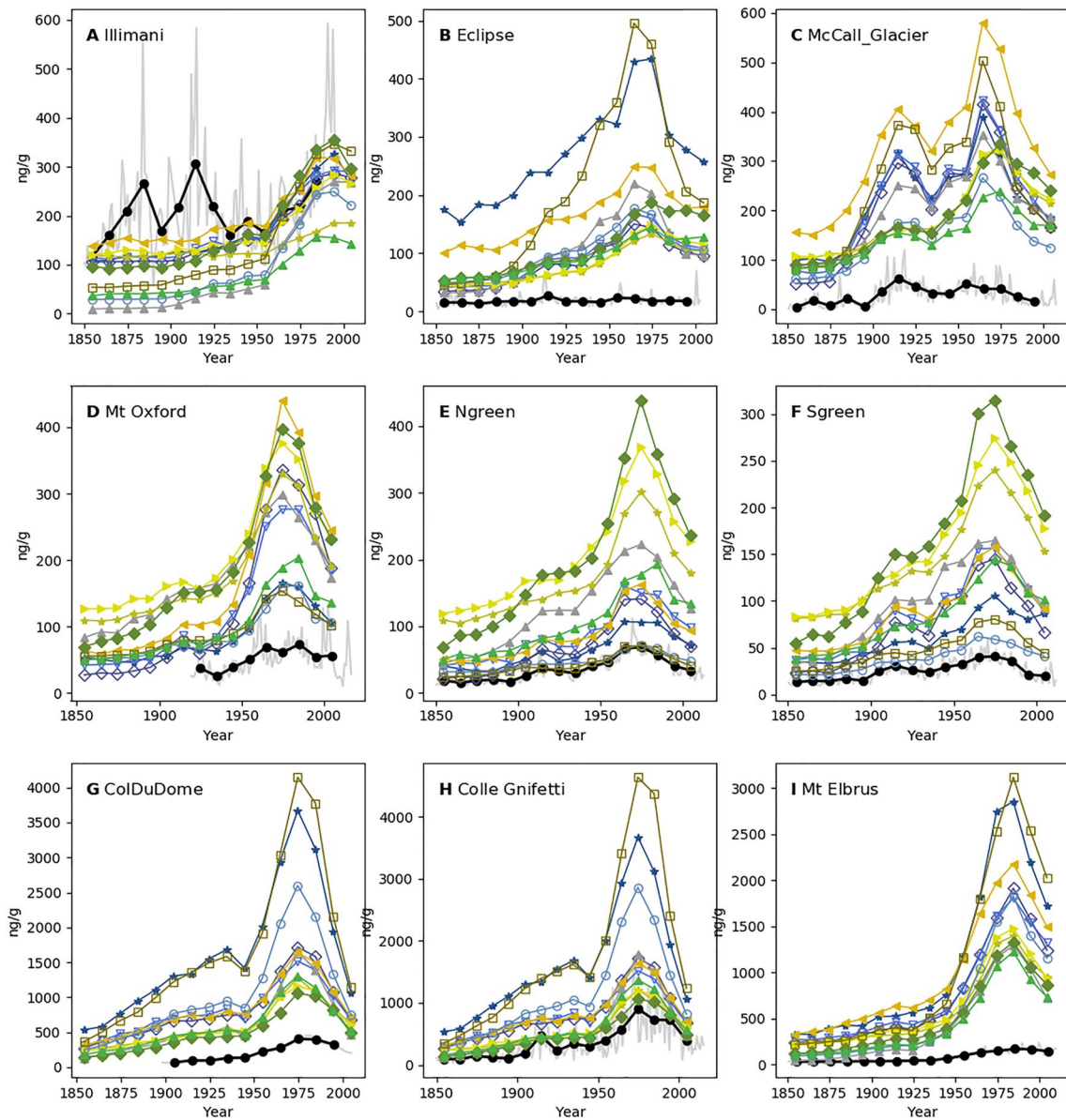


Figure B2. Sulfate concentrations for the ice core sites shown in Figure 1 per model. The legend can be seen in Figure C2.

Appendix C: Lifetimes of BC and Sulfate

See Figures C1 and C2.

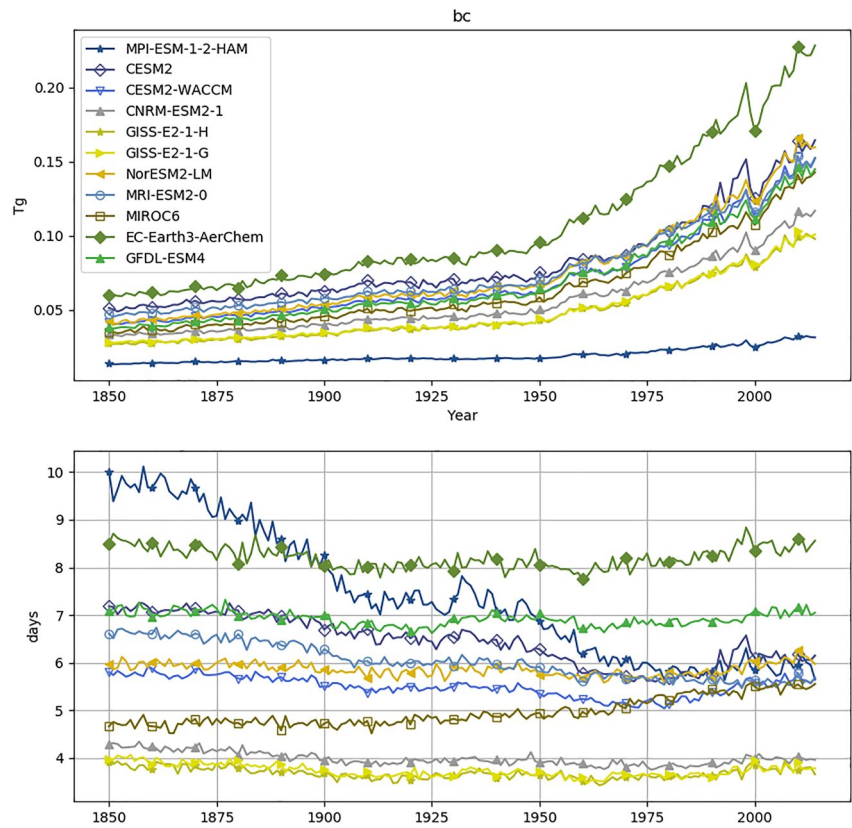


Figure C1. Global load and lifetime for sulfate. The model CESM2-WACCM has been removed from this figure as it is the only model containing volcanic emissions of sulfur dioxide, which drastically affects loads and lifetime for sulfate in this model.

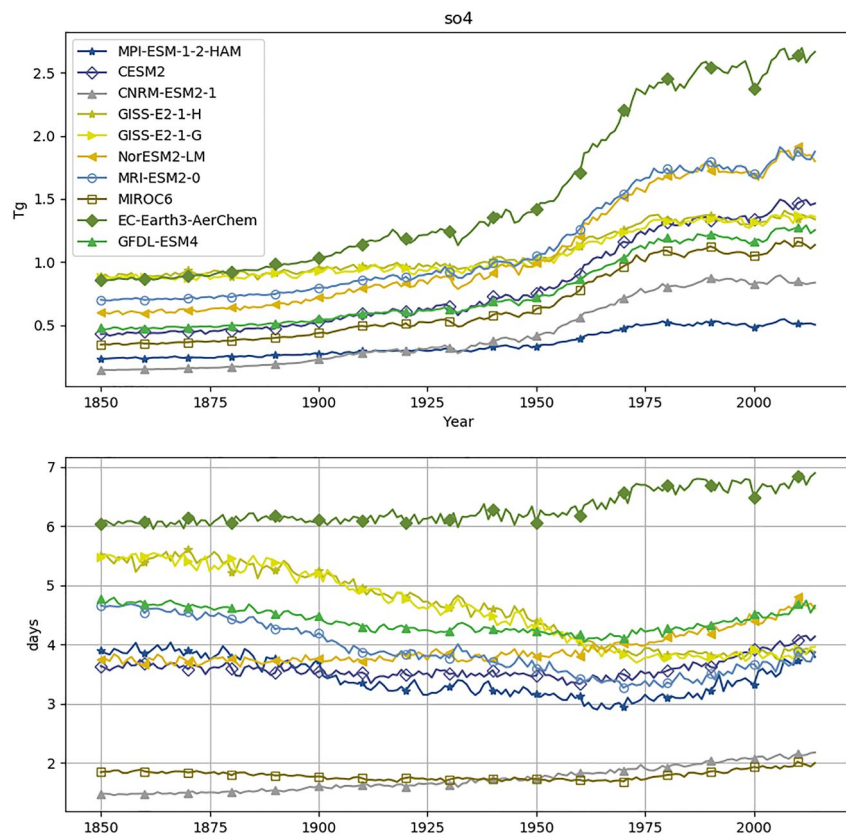


Figure C2. Global load and lifetime for black carbon.

Conflict of Interest

The authors declare no conflicts of interest relevant to this study.

Data Availability Statement

CMIP6 model outputs are freely available from the World Climate Research Programme (WCRP), 2011; <https://esgf-node.llnl.gov/search/cmip6/> (WCRP, 2021). The previously published ice core data is available following references and DOI's presented in Table 1. The ice core data together with the NorESM2-LM experiments performed specifically for this study is found at <https://zenodo.org/10.5281/zenodo.6526845> (Moseid et al., 2022).

Acknowledgments

This study benefited greatly from the CMIP6 data infrastructure for handling and providing model data for analysis. Jan Griesfeller is thanked for data organization. High-performance computing and storage resources were provided by the Norwegian infrastructure for computational science (through projects NS2345K, NS9560K, and NS9252K) and the Norwegian Meteorological Institute. A special thanks to Dr. Saehee Lim for recalculating the Mt Elbrus black carbon data into annual means for the purpose of this study. Financial support. This research has been supported by the European Union's Horizon 2020 (FORCeS) (Grant No. 821205) and the Research Council of Norway (KeyClim) (Grant No. 295046).

References

- Allen, R. J., & Landuyt, W. (2014). The vertical distribution of black carbon in CMIP5 models: Comparison to observations and the importance of convective transport. *Journal of Geophysical Research: Atmospheres*, *119*(8), 4808–4835. <https://doi.org/10.1002/2014jd021595>
- Avak, S. E., Trachsel, J. C., Edebeli, J., Brüttsch, S., Bartels-Rausch, T., Schneebeli, M., et al. (2019). Melt-Induced fractionation of major ions and trace elements in an alpine snowpack. *Journal of Geophysical Research: Earth Surface*, *124*(7), 1647–1657. <https://doi.org/10.1029/2019JF005026>
- Bauer, S. E., Bausch, A., Nazarenko, L., Tsigaridis, K., Xu, B., Edwards, R., et al. (2013). Historical and future black carbon deposition on the three ice caps: Ice core measurements and model simulations from 1850 to 2100. *Journal of Geophysical Research: Atmospheres*, *118*(14), 7948–7961. <https://doi.org/10.1002/jgrd.50612>
- Bellouin, N., Quaas, J., Gryspeerdt, E., Kinne, S., Stier, P., Watson-Parris, D., et al. (2019). Bounding global aerosol radiative forcing of climate change. *Reviews of Geophysics*, *58*(1), e2019RG000660. <https://doi.org/10.1029/2019RG000660>
- Bender, F. A.-M. (2020). Aerosol forcing: Still uncertain, still relevant. *AGU Advances*, *1*(3), e2019AV000128. <https://doi.org/10.1029/2019AV000128>
- Boers, R., de Laat, A. T., Stein Zweers, D. C., & Dirksen, R. J. (2010). Lifting potential of solar-heated aerosol layers. *Geophysical Research Letters*, *37*(24). <https://doi.org/10.1029/2010GL045171>
- Bond, T. C., Doherty, S. J., Fahey, D. W., Forster, P. M., Berntsen, T., De Angelo, B. J., et al. (2013). Bounding the role of black carbon in the climate system: A scientific assessment. *Journal of Geophysical Research: Atmospheres*, *118*(11), 5380–5552. <https://doi.org/10.1002/jgrd.50171>

- Danabasoglu, G., Lamarque, J.-F., Bacmeister, J., Bailey, D. A., DuVivier, A. K., Edwards, J., et al. (2020). The community Earth system model version 2 (CESM2). *Journal of Advances in Modeling Earth Systems*, *12*(2), e2019MS001916. <https://doi.org/10.1029/2019MS001916>
- de Laat, A. T. J., Stein Zweers, D. C., Boers, R., & Tuinder, O. N. E. (2012). A solar escalator: Observational evidence of the self-lifting of smoke and aerosols by absorption of solar radiation in the February 2009 Australian Black Saturday plume. *Journal of Geophysical Research*, *117*(D4). <https://doi.org/10.1029/2011JD017016>
- Dunne, J. P., Horowitz, L. W., Adcroft, A. J., Ginoux, P., Held, I. M., John, J. G., et al. (2020). The GFDL Earth system model version 4.1 (GFDL-ESM 4.1): Overall coupled model description and simulation characteristics. *Journal of Advances in Modeling Earth Systems*, *12*(11), e2019MS002015. <https://doi.org/10.1029/2019MS002015>
- Eichler, A., Schwikowski, M., & Gäggeler, H. W. (2001). Meltwater-induced relocation of chemical species in Alpine firn. *Tellus B: Chemical and Physical Meteorology*, *53*(2), 192–203. <https://doi.org/10.3402/tellusb.v53i2.16575>
- Engardt, M., Simpson, D., Schwikowski, M., & Granat, L. (2017). Deposition of sulphur and nitrogen in Europe 1900–2050. Model calculations and comparison to historical observations. *Tellus B: Chemical and Physical Meteorology*, *69*(1), 1328945. <https://doi.org/10.1080/16000889.2017.1328945>
- Eyring, V., Bony, S., Meehl, G. A., Senior, C. A., Stevens, B., Stouffer, R. J., & Taylor, K. E. (2016). Overview of the coupled model inter-comparison project Phase 6 (CMIP6) experimental design and organization. *Geoscientific Model Development*, *9*(5), 1937–1958. <https://doi.org/10.5194/gmd-9-1937-2016>
- Fagerli, H., Legrand, M., Preunkert, S., Vestreng, V., Simpson, D., & Cerqueira, M. (2007). Modeling historical long-term trends of sulfate, ammonium, and elemental carbon over Europe: A comparison with ice core records in the Alps. *Journal of Geophysical Research*, *112*(D23), D23S13. <https://doi.org/10.1029/2006JD008044>
- Forster, P., Storelvmo, T., Armour, K., Collins, W., Dufresne, J.-L., Frame, D., et al. (2021). The Earth's energy budget, climate feedbacks, and climate sensitivity. In V. Masson-Delmotte, P. Zhai, A. Pirani, S. L. Connors, C. Péan, S. Berger, et al. (Eds.) *Climate change 2021: The physical science basis. Contribution of working group I to the sixth assessment report of the intergovernmental panel on climate change*. Cambridge University Press. (pp. 923–1054). <https://doi.org/10.1017/9781009157896.009>
- Forster, P. M., Richardson, T., Maycock, A. C., Smith, C. J., Samset, B. H., Myhre, G., et al. (2016). Recommendations for diagnosing effective radiative forcing from climate models for CMIP6. *Journal of Geophysical Research: Atmospheres*, *121*(20), 12460–12475. <https://doi.org/10.1002/2016JD025320>
- Galmarini, S., Koffi, B., Solazzo, E., Keating, T., Hogrefe, C., Schulz, M., et al. (2017). Technical note: Coordination and harmonization of the multi-scale, multi-model activities HTAP2, AQMEII3, and MICS-Asia3: Simulations, emission inventories, boundary conditions, and model output formats. *Atmospheric Chemistry and Physics*, *17*(2), 1543–1555. <https://doi.org/10.5194/acp-17-1543-2017>
- Hodnebrog, O., Myhre, G., & Samset, B. H. (2014). How shorter black carbon lifetime alters its climate effect. *Nature Communications*, *5*(1), 5065. <https://doi.org/10.1038/ncomms6065>
- Hoesly, R. M., Smith, S. J., Feng, L., Klimont, Z., Janssens-Maenhout, G., Pitkanen, T., et al. (2018). Historical (1750–2014) anthropogenic emissions of reactive gases and aerosols from the Community Emissions Data System (CEDS). *Geoscientific Model Development*, *11*(1), 369–408. <https://doi.org/10.5194/gmd-11-369-2018>
- Kellerhals, T., Brüttsch, S., Sigl, M., Knüsel, S., Gäggeler, H. W., & Schwikowski, M. (2010). Ammonium concentration in ice cores: A new proxy for regional temperature reconstruction? *Journal of Geophysical Research*, *115*(D16), D16123. <https://doi.org/10.1029/2009JD012603>
- Kelley, M., Schmidt, G. A., Nazarenko, L. S., Bauer, S. E., Ruedy, R., Russell, G. L., et al. (2020). GISS-E2.1: Configurations and climatology. *Journal of Advances in Modeling Earth Systems*, *12*(8), e2019MS002025. <https://doi.org/10.1029/2019MS002025>
- Lamarque, J.-F., Bond, T. C., Eyring, V., Granier, C., Heil, A., Klimont, Z., et al. (2010). Historical (1850–2000) gridded anthropogenic and biomass burning emissions of reactive gases and aerosols: Methodology and application. *Atmospheric Chemistry and Physics*, *10*(15), 7017–7039. <https://doi.org/10.5194/acp-10-7017-2010>
- Legrand, M., Hammer, C., De Angelis, M., Savarino, J., Delmas, R., Clausen, H., & Johnsen, S. J. (1997). Sulfur-containing species (methanesulfonate and SO₂) over the last climatic cycle in the Greenland Ice Core Project (central Greenland) ice core. *Journal of Geophysical Research*, *102*(C12), 26663–26679. <https://doi.org/10.1029/97JC01436>
- Legrand, M., McConnell, J. R., Preunkert, S., Arienzo, M., Chellman, N., Gleason, K., et al. (2018). Alpine ice evidence of a three-fold increase in atmospheric iodine deposition since 1950 in Europe due to increasing oceanic emissions. *Proceedings of the National Academy of Sciences*, *115*(48), 12136–12141. <https://doi.org/10.1073/pnas.1809867115>
- Legrand, M., Preunkert, S., May, B., Guilhermet, J., Hoffman, H., & Wagenbach, D. (2013). Major 20th century changes of the content and chemical speciation of organic carbon archived in Alpine ice cores: Implications for the long-term change of organic aerosol over Europe. *Journal of Geophysical Research: Atmospheres*, *118*(9), 3879–3890. <https://doi.org/10.1002/jgrd.50202>
- Lim, S., Faïn, X., Ginot, P., Mikhalenko, V., Kutuzov, S., Paris, J.-D., et al. (2017). Black carbon variability since preindustrial times in the eastern part of Europe reconstructed from Mt. Elbrus, Caucasus, ice cores. *Atmospheric Chemistry and Physics*, *17*(5), 3489–3505. <https://doi.org/10.5194/acp-17-3489-2017>
- Liu, P., Kaplan, J. O., Mickley, L. J., Li, Y., Chellman, N. J., Arienzo, M. M., et al. (2020). Improved estimates of preindustrial biomass burning reduce the magnitude of aerosol climate forcing in the Southern Hemisphere. *Science Advances*, *7*(22), eabc1379. <https://doi.org/10.1126/sciadv.abc1379>
- Lohmann, U. (2017). Why does knowledge of past aerosol forcing matter for future climate change? *Journal of Geophysical Research: Atmospheres*, *122*(9), 5021–5023. <https://doi.org/10.1002/2017JD026962>
- Lohmann, U., & Feichter, J. (2005). Global indirect aerosol effects: A review. *Atmospheric Chemistry and Physics*, *5*(3), 715–737. <https://doi.org/10.5194/acp-5-715-2005>
- Mauritsen, T., Bader, J., Becker, T., Behrens, J., Bittner, M., Brokopf, R., et al. (2019). Developments in the MPI-M Earth system model version 1.2 (MPI-ESM1.2) and its response to increasing CO₂. *Journal of Advances in Modeling Earth Systems*, *11*(4), 998–1038. <https://doi.org/10.1029/2018MS001400>
- McConnell, J. R. (2010). New Directions: Historical black carbon and other ice core aerosol records in the Arctic for GCM evaluation. *Atmospheric Environment*, *44*(21), 2665–2666. <https://doi.org/10.1016/j.atmosenv.2010.04.004>
- McConnell, J. R., Burke, A., Dunbar, N. W., Köhler, P., Thomas, J. L., Arienzo, M. M., et al. (2017). Synchronous volcanic eruptions and abrupt climate change ca17.7 ka plausibly linked by stratospheric ozone depletion. *Proceedings of the National Academy of Sciences*, *114*(38), 10035–10040. <https://doi.org/10.1073/pnas.1705595114>
- McConnell, J. R., & Edwards, R. (2008). Coal burning leaves toxic heavy metal legacy in the Arctic. *Proceedings of the National Academy of Sciences*, *105*(34), 12140–12144. <https://doi.org/10.1073/pnas.0803564105>
- McConnell, J. R., Edwards, R., Kok, G. L., Flanner, M. G., Zender, C. S., Saltzman, E. S., et al. (2007). 20th century industrial black carbon emissions altered and climate forcing. *Science*, *317*(5843), 1381–1384. <https://doi.org/10.1126/science.1144856>

- Moseid, K. O., Schulz, M., Eichler, A., Schwikowski, M., McConnell, J., Olivie, D., et al. (2022). Ice core and model data for Moseid et al. 2022 [Dataset]. Zenodo. <https://doi.org/10.5281/zenodo.6526845>
- Moseid, K. O., Schulz, M., Storelvmo, T., Julsrud, I. R., Olivie, D., Nabat, P., et al. (2020). Bias in CMIP6 models as compared to observed regional dimming and brightening. *Atmospheric Chemistry and Physics*, 20(24), 16023–16040. <https://doi.org/10.5194/acp-20-16023-2020>
- Ohneiser, K., Ansmann, A., Chudnovsky, A., Engelmann, R., Ritter, C., Veselovskii, I., et al. (2021). The unexpected smoke layer in the High Arctic winter stratosphere during MOSAiC 2019–2020. *Atmospheric Chemistry and Physics*, 21(20), 15783–15808. <https://doi.org/10.5194/acp-21-15783-2021>
- Osmont, D., Sigl, M., Eichler, A., Jenk, T. M., & Schwikowski, M. (2019). A Holocene black carbon ice-core record of biomass burning in the Amazon Basin from Illimani, Bolivia. *Climate of the Past*, 15(2), 579–592. <https://doi.org/10.5194/cp-15-579-2019>
- Preunkert, S., Legrand, M., Kutuzov, S., Ginot, P., Mikhalenko, V., & Friedrich, R. (2019). The Elbrus (Caucasus, Russia) ice core record—Part 1: Reconstruction of past anthropogenic sulfur emissions in South-Eastern Europe. *Atmospheric Chemistry and Physics*, 19(22), 14119–14132. <https://doi.org/10.5194/acp-19-14119-2019>
- Preunkert, S., Legrand, M., & Wagenbach, D. (2001). Sulfate trends in a Col du Dôme (French Alps) ice core: A record of anthropogenic sulfate levels in the European midtroposphere over the twentieth century. *Journal of Geophysical Research*, 106(D23), 31991–32004. <https://doi.org/10.1029/2001JD000792>
- Schulz, M., Textor, C., Kinne, S., Balkanski, Y., Bauer, S., Bernsten, T., et al. (2006). Radiative forcing by aerosols as derived from the AeroCom present-day and pre-industrial simulations. *Atmospheric Chemistry and Physics*, 6(12), 5225–5246. <https://doi.org/10.5194/acp-6-5225-2006>
- Séférian, R., Nabat, P., Michou, M., Saint-Martin, D., Voldoire, A., Colin, J., et al. (2019). Evaluation of CNRM Earth system model, CNRM-ESM2-1: Role of Earth system processes in present-day and future climate. *Journal of Advances in Modeling Earth Systems*, 11(12), 4182–4227. <https://doi.org/10.1029/2019MS001791>
- Seland, O., Berntsen, M., Seland Graff, L., Olivie, D., Toniazzo, T., Gjermundsen, A., et al. (2020). The Norwegian Earth system model, NorESM2—Evaluation of the CMIP6 DECK and historical and scenario simulations. *Geoscientific Model Development Discussions*, 13(12), 1–68. <https://doi.org/10.5194/gmd-2019-378>
- Sherwood, S. C., Webb, M. J., Annan, J. D., Armour, K. C., Forster, P. M., Hargreaves, J. C., et al. (2020). An assessment of Earth's climate sensitivity using multiple lines of evidence. *Reviews of Geophysics*, 58(4), e2019RG000678. <https://doi.org/10.1029/2019RG000678>
- Sigl, M., Abram, N. J., Gabrieli, J., Jenk, T. M., Osmont, D., & Schwikowski, M. (2018). 19th century glacier retreat in the Alps preceded the emergence of industrial black carbon deposition on high-alpine glaciers. *The Cryosphere*, 12(10), 3311–3331. <https://doi.org/10.5194/tc-12-3311-2018>
- Sigl, M., McConnell, J. R., Layman, L., Maselli, O., McGwire, K., Pasteris, D., et al. (2013). A new bipolar ice core record of volcanism from WAIS Divide and NEM and implications for climate forcing of the last 2000 years. *Journal of Geophysical Research: Atmospheres*, 118(3), 1151–1169. <https://doi.org/10.1029/2012JD018603>
- Sigl, M., McConnell, J. R., Toohey, M., Curran, M., Das, S. B., Edwards, R., et al. (2014). Insights from Antarctica on volcanic forcing during the common era. *Nature Climate Change*, 4(8), 693–697. <https://doi.org/10.1038/nclimate2293>
- Sigl, M., Winstrup, M., McConnell, J. R., Welten, K. C., Plunkett, G., Ludlow, F., et al. (2015). Timing and climate forcing of volcanic eruptions for the past 2,500 years. *Nature*, 523(7562), 543–549. <https://doi.org/10.1038/nature14565>
- Storelvmo, T., Leirvik, T., Lohmann, U., Phillips, P. C. B., & Wild, M. (2016). Disentangling greenhouse warming and aerosol cooling to reveal Earth's climate sensitivity. *Nature Geoscience*, 9(4), 286–289. <https://doi.org/10.1038/ngeo2670>
- Szopa, S., Naik, V., Adhikary, B., Artaxo Netto, P. E., Berntsen, T., Collins, W. D., et al. (2021). Short-lived climate forcers. In V. Masson-Delmotte, P. Zhai, A. Pirani, S. L. Connors, C. Péan, S. Berger, N. Caud, et al. (Eds.). *Climate change 2021: The physical science basis. Contribution of working group I to the sixth assessment report of the intergovernmental panel on climate change*. Cambridge University Press. (pp. 817–922). <https://doi.org/10.1017/9781009157896.008>
- Tatebe, H., Ogura, T., Nitta, T., Komuro, Y., Ogochi, K., Takemura, T., et al. (2019). Description and basic evaluation of simulated mean state, internal variability, and climate sensitivity in MIROC6. *Geoscientific Model Development*, 12(7), 2727–2765. <https://doi.org/10.5194/gmd-12-2727-2019>
- Tegen, I., Neubauer, D., Ferrachat, S., Siegenthaler-Le Drian, C., Bey, I., Schutgens, N., et al. (2019). The global aerosol–climate model ECHAM6.3–HAM2.3 – Part 1: Aerosol evaluation. *Geoscientific Model Development*, 12(4), 1643–1677. <https://doi.org/10.5194/gmd-12-1643-2019>
- van Marle, M. J. E., Kloster, S., Magi, B. I., Marlon, J. R., Daniau, A.-L., Field, R. D., et al. (2017). Historic global biomass burning emissions for CMIP6 (BB4CMIP) based on merging satellite observations with proxies and fire models (1750–2015). *Geoscientific Model Development*, 10(9), 3329–3357. <https://doi.org/10.5194/gmd-10-3329-2017>
- van Noije, T., Bergman, T., Le Sager, P., O'Donnell, D., Makkonen, R., Gonçalves-Ageitos, M., et al. (2021). EC-Earth3-AerChem: A global climate model with interactive aerosols and atmospheric chemistry participating in CMIP6. *Geoscientific Model Development*, 14(9), 5637–5668. <https://doi.org/10.5194/gmd-14-5637-2021>
- WCRP (2021). *Coupled model intercomparison project, phase 6 (CMIP6) data*. World Climate Research Programme. Retrieved from <https://esgf-node.llnl.gov/search/cmip6>
- Wendl, I. A., Menking, J. A., Färber, R., Gysel, M., Kaspari, S. D., Laborde, M. J. G., & Schwikowski, M. (2014). Optimized method for black carbon analysis in ice and snow using the Single Particle Soot Photometer. *Atmospheric Measurement Techniques*, 7(8), 2667–2681. <https://doi.org/10.5194/amt-7-2667-2014>
- Yalcin, K., & Wake, C. P. (2001). Anthropogenic signals recorded in an ice core from Eclipse Icefield, Yukon Territory, Canada. *Geophysical Research Letters*, 28(23), 4487–4490. <https://doi.org/10.1029/2001GL013037>
- Yukimoto, S., Kawai, H., Koshiro, T., Oshima, N., Yoshida, K., Urakawa, S., et al. (2019). The meteorological research Institute Earth system model version 2.0, MRI-ESM2.0: Description and basic evaluation of the physical component. *Journal of the Meteorological Society of Japan. Ser. II*, 97(5), 931–965. <https://doi.org/10.2151/jmsj.2019-051>
- Zennaro, P., Kehrwald, N., McConnell, J. R., Schüpbach, S., Maselli, O. J., Marlon, J., et al. (2014). Fire in ice: Two millennia of boreal forest fire history from the Greenland NEM ice core. *Climate of the Past*, 10(5), 1905–1924. <https://doi.org/10.5194/cp-10-1905-2014>